Boosting Kidney Stone Identification in Endoscopic Images Using Two-Step Transfer Learning

Francisco Lopez-Tiro[1,2,3], Juan Pablo Betancur-Rengifo[3], Arturo Ruiz-Sanchez[3], Ivan Reyes-Amezcua[3,4],
Jonathan El-Beze[5], Jacques Hubert[5], Michel Daudon[6], Gilberto Ochoa-Ruiz*[,1,3], Christian Daul*[,2]

Abstract—Knowing the cause of kidney stone formation is crucial to establish treatments that prevent recurrence. There are currently different approaches for determining the kidney stone type. However, the reference ex-vivo identification procedure can take up to several weeks, while an in-vivo visual recognition requires highly trained specialists. Machine learning models have been developed to provide urologists with an automated classification of kidney stones during an ureteroscopy; however, there is a general lack in terms of quality of the training data and methods. In this work, a two-step transfer learning approach is used to train the kidney stone classifier. The proposed approach transfers knowledge learned on a set of images of kidney stones acquired with a CCD camera (ex-vivo dataset) to a final model that classifies images from endoscopic images (ex-vivo dataset). The results show that learning features from different domains with similar information helps to improve the performance of a model that performs classification in real conditions (for instance, uncontrolled lighting conditions and blur). Finally, in comparison to models that are trained from scratch or by initializing ImageNet weights, the obtained results suggest that the two-step approach extracts features improving the identification of kidney stones in endoscopic images.

Index Terms—Transfer learning, kidney stones, deep learning

I. INTRODUCTION

The formation of kidney stones in the urinary tract is a public health issue [1], [2]. In industrialized countries, 10% of the population suffers from an episode of kidney stones during their lifetime. Recent studies have determined that the risk of recurrence increases up to 40% in less than 5 years [3], [4]. Thus, determining the root cause of kidney stone formation is crucial to avoid relapses through personalized treatments [3], [5], [6]. Therefore, different approaches for visually identifying some of the most common types (or classes) of kidney stones have been proposed in recent years [7], [8].

The Morpho-Constitutional Analysis (MCA) is currently the reference method for the identification of the type of the extracted kidney stone fragments [9]. This ex-vivo procedure consists of two complementary analyses on the extracted kidney stone parts, which were fragmented with a laser.

The fragments are visually inspected under a microscope to observe the colors and textures of their surface and section. Then, an infrared-spectrophotometry analysis enables to identify the molecular and crystalline composition of the different areas (layers) of the kidney stone [10]. However, in numerous hospitals the MCA results are only available after some weeks. This delay makes it difficult to establish an immediate and appropriate treatment for the patient. On the other hand, removing large kidney stone fragments is often difficult in practice. Moreover, the biochemical composition can be altered by the laser during the fragmentation [11], making the MCA procedure challenging in some cases.

Endoscopic Stone Recognition (ESR) is a promising technique to immediately determine the type of kidney stones during the ureteroscopy (i.e., in-vivo recognition). The advantage of ESR is twice: kidney stones can be pulverized (dusting procedure with a laser) instead fragmented, and an appropriate treatment can be immediately defined. ESR is only based on a visual inspection of in-vivo endoscopic images observed on a screen. For trained urologists, ESR results are strongly correlated with those of MCA [12]. However, only a few highly trained experts are nowadays able to recognize the type of kidney stones using only endoscopic images. Moreover, the visual classification by urologists is operator dependent and subjective, and the required experience is long to acquire [13].

Studies have been recently proposed to automate ESR [12], [14], [15]. These Deep Learning (DL) based methods led to promising results. However, one of the most common challenges in these DL-based methods for classifying kidney stones is the lack of a large image set for the model training. In addition, the similarity of the data distribution is another important factor to obtain an adequate model. Consequently, this suggests a trade-off between the amount of available data and the data distribution to fit the network weights adequately. The majority of the DL-based models report fine-tuning of weights learned from distributions other than those from kidney stone images (commonly from ImageNet [16]).

Transfer Learning (TL) is used when features learned from a given domain (or class of images) can bring appropriate knowledge to another domain for which the available image set is too small to train a large model from scratch [17], [22]. In the context of ureteroscopy, a large dataset of in-vivo images is currently not available and collecting such a large database of endoscopic images during ureteroscopies is a long term work. However, in the context of this work, images of ex-vivo

[1]Tecnologico de Monterrey, School of Sciences and Engineering, Mexico
[2]CRAN (UMR 7039, Université de Lorraine and CNRS), Nancy, France
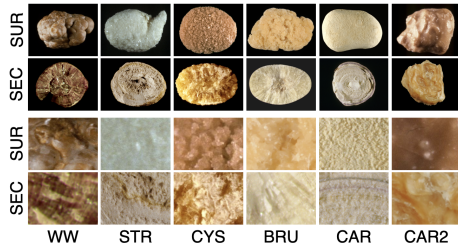[3]CV-INSIDE Lab Member, Mexico
[4]CINVESTAV, Computer Sciences Department, Mexico
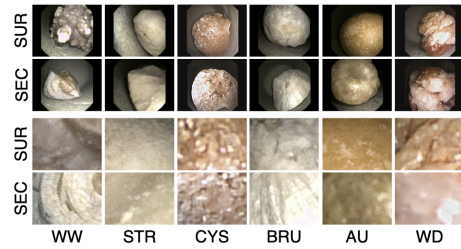[5]CHU Nancy, Service d'urologie de Brabois, Vandœuvre-lès-Nancy, France
[6]Hôpital Tenon, AP-HP, Paris, France
*Corresponding authors:
gilberto.ochoa@tec.mx, christian.daul@univ-lorraine.fr

(a) Dataset A: CCD-camera images (ex-vivo)

(b) Dataset B: Endoscopic images (ex-vivo)

Fig. 1: Examples of ex-vivo kidney stone images acquired with (a) a CCD camera [9] and (b) an endoscope [18]. SEC and SUR stand for section and surface views, respectively. The class types (WW, STR, CYS, etc.) are defined in Table I.

kidney stone fragments (acquired with standard CCD cameras) are available. Due to their similarity in color, texture and morphological features, TL can be used to distill knowledge from CCD-camera images into the final classifier of the images acquired with endoscopes.

Based on this idea, a two-step TL model to classify six types of kidney stones is proposed. The model uses a homogeneous, as well as a heterogeneous TL phase on a ResNet50 architecture pre-trained with the ImageNet dataset. To validate our proposal, the approach transfers knowledge learned on a small set of images acquired with classical CCD cameras to a final model that classifies ex-vivo endoscopic images.

The rest of this paper is organized as follows. Section II provides an overview of the ex-vivo datasets, namely the CCD (digital) camera image and endoscopic image sets. Section II also presents the two-step TL approach. Section III compares the performances of the two-step TL approach with those of the methods of the literature. Finally, Section IV concludes this contribution and proposes perspectives.

II. MATERIALS AND METHODS

A. Datasets

Two kidney stone datasets were used in our experiments (see Table I): images were acquired with standard CCD cameras, and endoscopic images were captured with an ureteroscope. The dataset's main characteristics are described below.

Dataset A, [9]. This ex-vivo dataset of 366 CCD camera images (see the two upper lines in Fig. 1a) is split in 209 surface and 157 section images, and contains six different stone types sorted by sub-types denoted by WW (Whewellite, sub-type Ia), CAR (Carbapatite, IVa), CAR2 (Carbapatite, IVa2), STR (Struvite, IVc), BRU (Brushite, IVd) and CYS (Cystine, Va). The fragment images were acquired with a digital camera under controlled lighting conditions and with a uniform background.

Dataset B, [18]. The endoscopic dataset consists of 409 images (see the two upper lines in Fig. 1b). This dataset includes 246 surface and section 163 images. Dataset B involves the same classes as dataset A, except that the carbatite stones (sub-types IVa1 and IVa2) are replaced by the weddelite (sub-type IIa) and uric acid (IIIa) classes. The images of dataset B were captured with an endoscope by placing kidney

TABLE I: Description of the two ex-vivo datasets.

Dataset A (M. Corrales et al. [9])

Subtype	Main component	Key	Surface	Section	Mixed
Ia	Whewellite	WW	50	74	124
IVa1	Carbapatite	CAR	18	18	36
IVa2	Carbapatite	CAR2	36	18	54
IVc	Struvite	STR	25	19	44
IVd	Brushite	BRU	43	17	60
Va	Cystine	CYS	37	11	48
		TOTAL	209	157	366

Dataset B (J. El-Beze et al. [18])

Subtype	Main component	Key	Surface	Section	Mixed
Ia	Whewellite	WW	62	25	87
IIa	Weddellite	WD	13	12	25
IIIa	Acide Urique	AU	58	50	108
IVc	Struvite	STR	43	24	67
IVd	Brushite	BRU	23	4	27
Va	Cystine	CYS	47	48	95
		TOTAL	246	163	409

stone fragments in an environment simulating in a realistic way the shape and color or ureters (for more details see [18]). These images are visually close to in-vivo images since the fragments were acquired with an ureteroscope and by simulating a quite realistic the clinical in-vivo scenes.

Due to the small size of the two datasets, and due to their class imbalance, patches were extracted from the images to increase and balance the number of training and testing samples. The two last lines of Figs. 1a and 1b show such patches. As demonstrated in previous works [15], [19], [20], the use of square patches of appropriate size allows to capture sufficient color and texture information for the classification. In addition, the use of patches instead of full surface and section images allows for augmenting and balancing the datasets. According to [20], a patch size of 256×256 pixels was chosen for the A and B datasets. A patch overlap of at most 20 pixels is set to avoid redundant information inside the image of a same kidney stone fragment. A total of 12,000 patches were extracted, both for dataset A and dataset B.

The patches of each dataset were "whitened" using the mean m_i and standard deviation σ_i of the color values I_i^w for each RGB channel with $I_i^w = (I_i - m_i)/\sigma_i$, with i = R, G, B. To avoid data leakage in the datasets, a random, non-repeating
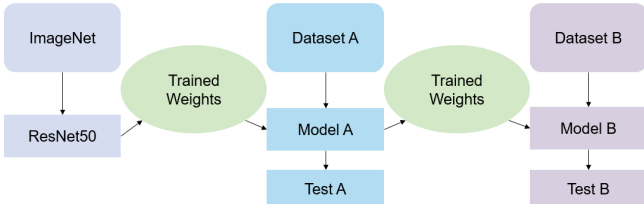
Fig. 2: Two-step TL workflow. Model A was first initialized with the weights of a ResNet50 network pre-trained with ImageNet, and then fine-tuned with Dataset A. Next, Model B starts with the weights learned from Model A and is finally fine-tuned with Dataset B.

dataset partitioning strategy was used (in contrast to previous works that used repeated images in both sets). 80% of the data was used for training and 20% for testing.

B. Two-step transfer learning

Depending on the difference between two image domains, TL can be classified into homogeneous and heterogeneous transfer techniques. Homogeneous TL (HoTL) is applicable when specific datasets relating to a particular domain are available, even if the later is only "similar" to the images of the target domain (i.e., the dataset from which the knowledge is transferred does not exactly match the target dataset, but carries similar information). On the other hand, heterogeneous TL (HeTL) is the case where the datasets of the source and target domains differ [21], [22]. Furthermore, when a reduced amount of training data is available, it is recommended to initialize the weights of architectures with pre-trained values rather than random values (i.e., TL from the scratch) [22]. Thus, in the first step of the proposed two-step strategy, a large dataset (ImageNet) is used to transfer knowledge into a network (ResNet50) which is fine-tuned by the smaller kidney stone image set acquired under controlled acquisition conditions (dataset A). After this HeTL step, an HoTL is used, this second step exploiting dataset B including endoscopic images close to dataset A, but with more image quality variability as really encountered in ureteroscopy.

First TL step: HeTL. Figure 2 shows the workflow of the two-step TL process. The first step is the heterogeneous phase in which the weights are initialized. To do so, a ResNet50 architecture was pre-trained with ImageNet [16] and used to train a model able to classify the six types of kidney stones from dataset A (see Table I).

In this HeTL step, Gaussian blur and geometrical transformations are only applied to the training images with the aim of preparing the model for dataset B. A batch size of 24 was used along with a SGD optimizer with a learning rate of 0.001 and momentum of 0.9. Fully connected layers with 768,256,128 and 6 neurons were added with batch-normalization, ReLU activation function, and a dropout of 0.5.

Second TL-step: HoTL. The homogeneous learning occurs in the second step of the TL-process. It consists in transferring the knowledge (weights) of the trained model from the HeTL into dataset B to differentiate between the six types of kidney

stones that are in this dataset (see Table I). The initial weights of model B are those after the fine-tuning of model A with dataset A, model B being finally fine-tuned with dataset B. The purpose of this approach is to improve the generalization performance of model B and facilitate the extraction of robust features [23]. Here, only geometric transformations were applied to the patches, since the image quality variability in dataset B is naturally high, while this variability is limited in dataset A. Moreover, 30 epochs were also executed with a SGD optimizer, but with a larger learning rate of 0.01 since it was expected that the model had less to learn. However, fully connected layers were not added since the idea was to use the trained model without further modifications to the architecture.

III. RESULTS AND DISCUSSION

Three different experiments were carried out to assess the performance of the two-step TL approach presented in Section II-B using patch data described in Section II-A. The ability of the two-step TL approach (see Fig. 2) to predict kidney stone types on endoscopic and digital camera images was evaluated with surface (first experiment) and section patches (second experiment), these patch types being separately used. In the third experiment, based on a "mixed" dataset, the performance of the two-step TL approach was evaluated by simultaneously using surface and section patches. In previous works based on DL [15], [19], [20] it has been reported that the combination of kidney stone patch types improves the classification process over models trained with only one patch type. Furthermore, mixing patch types closely simulates the way experts perform MCA and ESR [9], [10]. The results of our experiments are summarized in Table II and discussed below.

A. Two step TL-approach results

Experiment 1. From the surface patch results, it can be seen that the weights heterogeneously transferred from ResNet50 to model A (the "HeTL only" strategy applied on dataset A, see Table II) led to an accuracy of 0.649±0.050) is useful to avoid training the model from scratch (accuracy of 0.582±0.033 for the "No TL" strategy applied on dataset A). Although the performance of "HeTL only" remains low, it is also noticeable that the two-step TL strategy ("HeTL+HoTL") of Fig. 2 improves significantly the identification performance, obtaining an overall accuracy over 6 classes of 0.832±0.012 (increase of 18% compared the "HeTL only" strategy with dataset A). The accuracy increase from "HeTL only" to the "HeTL+HoTL" strategy is due to the similarity of the colors and textures of kidney stone fragments in databases A and B.

Experiment 2. For section patches, the results of "HeTL only" applied on dataset A are promising (accuracy of 0.824±0.022). This high performance was reached due to the rich textural information in section patches which is not present in surface images. An accuracy of 0.904±0.048 was obtained for "HeTL+HoTL" applied on dataset B. Although the 8% increase from "HeTL only" to the "HeTL+HoTL" strategy was smaller for section data as for surface patches, this accuracy was the highest one in all three experiments.

TABLE II: Mean ± standard deviation determined for each metric quantifying the results for each patch type set (fragment surface patches, section patches, and both patch types mixed) and for various TL-strategies after 5 executions. Accuracy, Precision, Recall, and F1-Score were used to measure over six classes the performance of the models for each TL-strategy.

| Patch type	TL strategy	Accuracy	Precision	Recall	F1-Score	Dataset	Training details
Surface	No TL	0.582±0.033	0.588±0.028	0.582±0.033	0.579±0.028	A	Baseline (no TL) trained on dataset A
	No TL	0.702±0.012	0.718±0.010	0.702±0.012	0.701±0.008	B	Baseline (no TL) trained on dataset B
	HeTL only	0.649±0.050	0.655±0.039	0.649±0.050	0.642±0.046	A	Baseline + TL with ImageNet weights
	HeTL only	0.820±0.033	0.833±0.029	0.820±0.033	0.818±0.032	B	Baseline + TL with ImageNet weights
	HeTL + HoTL	**0.832±0.012**	**0.845±0.012**	**0.832±0.012**	**0.829±0.012**	**B**	**Baseline + TL with ImageNet + TL dataset A**
Section	No TL	0.592±0.039	0.627±0.029	0.592±0.039	0.596±0.039	A	Baseline (no TL) trained on dataset A
	No TL	0.738±0.022	0.772±0.015	0.738±0.022	0.722±0.023	B	Baseline (no TL) trained on dataset B
	HeTL only	0.824±0.022	0.834±0.020	0.824±0.022	0.820±0.023	A	Baseline + TL with ImageNet weights
	HeTL only	0.873±0.041	0.897±0.021	0.873±0.041	0.872±0.043	B	Baseline + TL with ImageNet weights
	HeTL + HoTL	**0.904±0.048**	**0.915±0.037**	**0.904±0.048**	**0.903±0.050**	**B**	**Baseline + TL with ImageNet + TL dataset A**
Mixed	No TL	0.594±0.021	0.610±0.023	0.594±0.021	0.596±0.020	A	Baseline (no TL) trained on dataset A
	No TL	0.760±0.024	0.773±0.029	0.760±0.024	0.752±0.024	B	Baseline (no TL) trained on dataset B
	HeTL only	0.800±0.013	0.809±0.013	0.800±0.013	0.797±0.013	A	Baseline + TL with ImageNet weights
	HeTL only	0.837±0.032	0.848±0.030	0.837±0.032	0.834±0.035	B	Baseline + TL with ImageNet weights
	HeTL + HoTL	**0.856±0.001**	**0.868±0.002**	**0.856±0.001**	**0.854±0.001**	**B**	**Baseline + TL with ImageNet + TL dataset A**
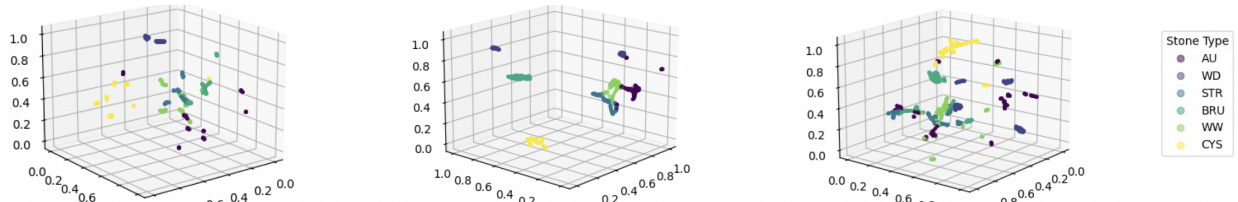
Fig. 3: UMAP-ICN dimensionality feature reduction [24]. From left to right: surface, section, and mixed patch sets. The visualizations were generated in the second step of the "HeTL+HoTL" strategy (see Fig. 2).

Experiment 3. The "HeTL" strategy applied on mixed patches of dataset A, led to an accuracy of 0.8±0.013. This performance in increased by 5% by the "HeTL+HoTL" strategy which has an accuracy of 0.856±0.001. In previous contributions it has been reported that the simulatneous use of surface and section led to the highest performance. This observation is not confirmed here, since the best results were obtained for section patches in experiment 2.

Table II shows that, in comparison to a learning from scratch, all TL-strategies improve the values of all four performance criteria, whatever the dataset. The UMAP-ICN visualisation [24] of Fig. 3 represents the features extracted in the last step of the "HeTL+HoTL" strategy. It is visible that for all patch types, the inter-class distance is high and the intra-class distance is weak.

B. Comparison with the state-of-the-art

Table III details the performance of reference DL-based methods used to identify the type of kidney stones using endoscopic image patches. These methods were [12], [14], [19] were all implemented and evaluated on dataset B (endoscopic dataset), and compared to the TL-approach described in this contribution. The results demonstrate that the two-step TL model outperforms the solutions described in [12], [14], [19] in terms of accuracy. Thus, DL-strategies involving a pre-training with a general database, followed by a first tuning with a specific database, and ending with a final tuning with the target

TABLE III: Comparison of the performance of various kidney stone identification methods. The value of the accuracy over all classes was determined with dataset B for all methods.

Method	Surface	Section	Mixed
Martinez, et al. [19]	0.562±0.233	0.466±0.128	0.527±0.189
Black, et al. [14]	0.735±0.190	0.762±0.185	0.801±0.138
Estrade, et al. [12]	0.737±0.179	0.788±0.106	0.701±0.223
This contribution	**0.832±0.012**	**0.904±0.048**	**0.856±0.001**

database can effectively lead to an improved performance on different data distributions without the need of a large amount of data.

IV. CONCLUSION AND PERSPECTIVE

It was demonstrated that it is possible to classify six different types of kidney stones using a small datasets of endoscopic images, the strategy being first to pre-learn the model with images acquired under controlled acquisition conditions (CCD camera) and then to exploit a fine tuning of the model using images captured in conditions simulating in a realistic way an ureteroscopy. This study confirms that it is easier for a neural network to adjust the weights learned on similar distributions and adapt them to a multiple class task. It is desirable that models of this type should be adapted to identify kidney stones using the complete endoscopic images instead of patches. We believe that the proposed approach will facilitate training on

whole-image models when the datasets are reduced in the number of images.

COMPLIANCE WITH ETHICAL APPROVAL

The images were captured in medical procedures following the ethical principles outlined in the Helsinki Declaration of 1975, as revised in 2000, with the consent of the patients.

REFERENCES

[1] P. M. Hall, "Ephrolithiasis: treatment, causes, and prevention," Cleveland Clinic journal of medicine, vol. 76, pp. 583–591, 2009.

[2] G. P. Kasidas, C. T. Samuell, T. B. Weir, "Renal stone analysis: why and how?," Annals of clinical biochemistry, vol. 41, pp. 91–97, 2004.

[3] G. Kartha, J. C. Calle, G. S. Marchini, M. Monga, "Impact of stone disease: chronic kidney disease and quality of life," Urologic Clinics, vol. 40, pp. 135–147, 2013.

[4] C. D. Scales Jr, A. C. Smith, J. M. Hanley, C. S. Saigal, "Prevalence of kidney stones in the United States," European urology, vol. 62, pp. 160–165, 2012.

[5] J. I. Friedlander, J. A. Antonelli, M. S. Pearle, "Diet: from food to stone," World journal of urology, vol. 33, pp. 179–185, 2015.

[6] A. Viljoen, R. Chaudhry, J. Bycroft, "Renal stones," Annals of clinical biochemistry, vol. 56, pp. 15–27, 2019.

[7] M. Daudon, P. Jungers, "Clinical value of crystalluria and quantitative morphoconstitutional analysis of urinary calculi," Nephron Physiology, vol. 98, pp. 31–36, 2004.

[8] V. Estrade, M. Daudon, O. Traxer, P. Meria, "Why should urologist recognize urinary stone and how? The basis of endoscopic recognition," Progrès en Urologie, vol. 27, pp. 26–35, 2017.

[9] M. Corrales, S. Doizi, Y. Barghouthy, O. Traxer, M. Daudon, "Classification of stones according to Michel Daudon: a narrative review," European Urology Focus, vol. 7, pp. 12–21, 2021.

[10] M. Daudon, A. Dessombz, V. Frochot, E. Letavernier, J-P. Haymann, P. Jungers, D. Bazin, "Comprehensive morpho-constitutional analysis of urinary stones improves etiological diagnosis and therapeutic strategy of nephrolithiasis," Comptes Rendus Chimie, vol. 19, pp. 1470–1491, 2016.

[11] E. X. Keller, V. De Coninck, M. Audouin, S. Doizi, D. Bazin, M. Daudon, O. Traxer, "Fragments and dust after Holmium laser lithotripsy with or without "Moses technology": How are they different?," Journal of Biophotonics, vol. 12, pp.e201800227, 2019.

[12] V. Estrade, M. Daudon, E. Richard, J-C. Bernhard, F. Bladou, G. Robert, B. Denis de Senneville, "Towards automatic recognition of pure and mixed stones using intra-operative endoscopic digital images," BJU international, vol. 129, pp. 234–242, 2022.

[13] V. De Coninck, E. X. Keller, O. Traxer, "Metabolic evaluation: who, when and how often," Current Opinion in Urology, vol. 29, pp. 52–64, 2019.

[14] K. M. Black, H. Law, A. Aldoukhi, J. Deng, K. R. Ghani, "Deep learning computer vision algorithm for detecting kidney stone composition," BJU international, vol. 125, pp. 920–924, 2020.

[15] F. Lopez, A. Varelo, O. Hinojosa, M. Mendez, D-H. Trinh, Y. El-Beze, J. Hubert, V. Estrade, M. Gonzalez, G. Ochoa, C. Daul, "Assessing deep learning methods for the identification of kidney stones in endoscopic images," 2021 43rd Annual International Conference of the IEEE Engineering in Medicine & Biology Society (EMBC), pp. 2778–2781, 2021.

[16] J. Deng, W. Dong, R. Socher, L-J. Li, K. Li, L. Fei-Fei, "Imagenet: A large-scale hierarchical image database," 2009 IEEE conference on computer vision and pattern recognition, pp. 248–255, 2009.

[17] Y. Wen, L. Chen, C. Zhou, Y. Deng, H. Zeng, S. Xi, R. Guo, "On the Effective Transfer Learning Strategy for Medical Image Analysis in Deep Learning," 2020 IEEE International Conference on Bioinformatics and Biomedicine (BIBM), pp. 827–834, 2020.

[18] J. El-Beze, C. Mazeaud, C. Daul, G. Ochoa-Ruiz, M. Daudon, P. Eschwège, J. Hubert, "Evaluation and understanding of automated urinary stone recognition methods," BJU international, 2022.

[19] A. Martínez, D-H. Trinh, J. El-Beze, J. Hubert, P. Eschwege, V. Estrade, L. Aguilar, C. Daul, G. Ochoa, "Towards an automated classification method for ureteroscopic kidney stone images using ensemble learning," 2020 42nd Annual International Conference of the IEEE Engineering in Medicine & Biology Society (EMBC), pp. 1936–1939, 2020.

[20] G. Ochoa-Ruiz, V. Estrade, F. Lopez, D. Flores-Araiza, J. El-Beze, D-H. Trinh, M. Gonzalez-Mendoza, P. Eschwège, J. Hubert, C. Daul, "On the in vivo recognition of kidney stones using machine learning," arXiv preprint arXiv:2201.08865, 2022.

[21] F. Zhuang, Z. Qi, K. Duan, S. Xi, Y. Zhu, H. Zhu, H. Xiong, Q. He, "A comprehensive survey on transfer learning," Proceedings of the IEEE, vol. 109, pp. 43–76, 2020.

[22] M. Raghu, C. Zhang, J. Kleinberg, S. Bengio, "Transfusion: Understanding transfer learning for medical imaging," Advances in neural information processing systems, vol. 32, 2019.

[23] J. Yosinski, J. Clune, Y. Bengio, H. Lipson, "How transferable are features in deep neural networks?," Advances in neural information processing systems, vol. 27, 2014.

[24] M. Mendez-Ruiz, I. Garcia, J. Gonzalez-Zapata, G. Ochoa-Ruiz, A. Mendez-Vazquez, "Finding Significant Features for Few-Shot Learning Using Dimensionality Reduction," Advances in Computational Intelligence: 20th Mexican International Conference on Artificial Intelligence, pp. 131–142, 2021.